

Magnetized Atmospheres around Neutron Stars Accreting at Low Rates

Silvia Zane

Nuclear and Astrophysics Laboratory, University of Oxford,
Keble Road, Oxford OX1 3RH, England
e-mail: zane@astro.ox.ac.uk

Roberto Turolla

Dept. of Physics, University of Padova,
Via Marzolo 8, 35131 Padova, Italy
e-mail: turolla@pd.infn.it

and

Aldo Treves

Dept. of Sciences, University of Insubria,
Via Lucini 3, 22100, Como, Italy
e-mail: treves@uni.mi.astro.it

ABSTRACT

We present a detailed investigation of atmospheres around accreting neutron stars with high magnetic field ($B \gtrsim 10^{12}$ G) and low luminosity ($L \lesssim 10^{33}$ erg/s). We compute the atmospheric structure, intensity and emergent spectrum for a plane-parallel, pure hydrogen medium by solving the transfer equations for the normal modes coupled to the hydrostatic and energy balance equations. The hard tail found in previous investigations for accreting, non-magnetic neutron stars with comparable luminosity is suppressed and the X-ray spectrum, although still harder than a blackbody at the star effective temperature, is nearly planckian in shape. Spectra from accreting atmospheres, both with high and low fields, are found to exhibit a significant excess at optical wavelengths above the Rayleigh-Jeans tail of the X-ray continuum.

Subject headings: Accretion, accretion disks — radiative transfer — stars: magnetic fields — stars: neutron — X-rays: stars

1. Introduction

The problem of investigating the properties of radiation emitted by neutron stars (NSs) accreting at low rates, $\dot{M} \approx 10^{10} - 10^{14}$ g/s, became of interest after it was realized that the

Galaxy may contain a large population of low luminosity magnetic accretors (see e.g. Nelson, Wang, Salpeter, & Wasserman 1995). The Galaxy should harbor more than 10^3 Be/X-ray binaries with an accreting NS shining at $\approx 10^{32} - 10^{34}$ erg/s (Rappaport, & van den Heuvel 1982; van den Heuvel, & Rappaport 1986). Moreover, assuming a supernova birth rate of $10-100 \text{ yr}^{-1}$, $\sim 10^8 - 10^9$ old, isolated NSs (ONSs) should be present in the Galaxy. Accretion onto a strongly magnetized, moving neutron star may be severely hindered for different reasons, but there is the possibility that a small, albeit non-negligible, fraction of ONSs may be accreting directly from the interstellar medium and some of them might be above the sensitivity threshold of ROSAT (e.g. Treves, & Colpi 1991; Blaes, & Madau 1993; see Treves, Turolla, Zane, & Colpi 1999 for a review).

At variance with neutron stars accreting at high rates, e.g. in X-ray pulsators, in low-luminosity sources the interaction of the escaping radiation with the inflowing material is of little importance, so they provide a much simpler case for investigating the physics of accretion in a strongly magnetized environment. For luminosities far below the Eddington limit, the accretion problem becomes germane to that of calculating the spectrum emerging from static atmospheres around cooling NSs. Spectra from cooling NSs have been widely investigated by a number of authors in connection with the X-ray emission from young, millisecond pulsars and isolated NSs, both for low and high magnetic fields and for different chemical compositions (see e.g. Romani 1987; Shibanov, Zavlin, Pavlov & Ventura 1992; Rajagopal, & Romani 1996; Pavlov, Zavlin, Trümper, & Neuhäuser 1996). Emerging spectra are not very different from a blackbody at the star effective temperature, the distinctive hardening present at low fields ($B \lesssim 10^9 \text{ G}$) becoming less pronounced when the magnetic field is $\sim 10^{12} - 10^{13} \text{ G}$. Similar conclusions were reached for the spectrum emitted by low-luminosity, low-field, accreting NSs by Zampieri, Turolla, Zane, & Treves (1995, hereafter ZTZT) for a pure hydrogen atmospheric composition.

The search of isolated neutron stars with ROSAT produced in recent years half a dozen promising candidates (Walter, Wolk, & Neuhäuser 1996; Haberl *et al.* 1997; Haberl, Motch & Pietsch 1998; Schwope *et al.* 1999; Motch *et al.* 1999; Haberl, Pietsch & Motch 1999). All of them show a soft, thermal X-ray spectrum, with typical energies $\sim 100 \text{ eV}$, and have an exceedingly large X-ray to optical flux ratio, $\gtrsim 10^4$. Although their association with isolated neutron stars is firmly established, their interpretation in terms of an accreting or a cooling object is still a matter of lively debate. Present models predict rather similar spectral distributions in both cases, especially in the X-ray band. It is therefore of particular importance to improve our theoretical understanding of these two classes of sources, looking, in particular, for spectral signatures which can enable us to discriminate between them.

In this paper we present a first detailed calculation of spectra emitted by strongly magnetized ($B \gtrsim 10^{12} \text{ G}$), accreting neutron stars, focusing our attention on low luminosities, $L \sim 10^{30}-10^{33} \text{ erg/s}$, such as those expected from old neutron stars accreting the interstellar medium. Spectral distributions are computed solving the transfer equations for the normal modes coupled to the hydrostatic equilibrium and the energy balance for different values of the accretion rate and the magnetic field.

We find that spectra emerging from magnetized, accretion atmospheres are blackbody-like in the X-ray band, in close agreement with the known results for cooling, magnetized atmospheres. However, accretion spectra show a new and distinctive feature at low energies, being characterized by an excess over the Raleigh–Jeans tail of the X-ray continuum below ~ 10 eV. The same behaviour is found in accretion atmospheres around unmagnetized neutron stars, but, as already pointed out by ZTZT, the X-ray spectrum is sensibly harder in this case. This result may be relevant in connection with the isolated neutron star candidate RX J18563.5-3754. Multiwavelength observations of this source indicate that, while ROSAT data are well fitted by a blackbody at $T_{eff} \sim 60$ eV, HST points lie above the extrapolation of the fit in the optical (Walter, & Matthews 1997).

The plan of the paper is as follows. The input physics relevant to our model is presented in §2: radiative transfer in a magnetized plasma is discussed in §2.1 and the structure of an accreting, magnetized atmosphere in §2.2. Computed spectra are presented in §3. Discussion and conclusions follow in §4.

2. The Model

2.1. Radiation Transfer

In this paper we consider a magnetized, nondegenerate, pure hydrogen, cold plasma, in which the main radiative processes are free–free emission/absorption and Thomson scattering. The plasma is in local thermal equilibrium (LTE) at temperature T . We consider a plane-parallel geometry with normal \mathbf{n} parallel to the magnetic field \mathbf{B} and to the z -direction. The stratification of the atmosphere is described by using as a parameter the scattering depth τ , as defined for an unmagnetized medium

$$\tau = \kappa_{es} \int_z^\infty \rho dz \quad (1)$$

where z is the coordinate variable, ρ is the plasma density, $\kappa_{es} = \sigma_T/m_p$ is the Thomson opacity and σ_T is the Thomson cross section.

In the following, we neglect collective plasma effects and consider only the limit $\omega_p^2/\omega^2 \ll 1$, where $\omega_p = (4\pi n_e e^2/m_e)^{1/2}$ is the plasma frequency and n_e electron density. We also consider only frequencies lower than the electron cyclotron frequency, $\omega_{c,e} = eB/m_e c$, so the semitransverse approximation can be assumed to hold. Since, for $\tau \gtrsim 0.01$, the temperature in the atmosphere is always $\lesssim 10^7$ K (see §2.2 and ZTZT) and scattering dominates over true absorption only for $\tau \sim 1$, Comptonization is negligible. For this reason, similarly to what is done for cooling, magnetized atmospheres (see e.g. Shibanov, *et al.* 1992), only conservative scattering is accounted for in the transfer equations (see, however, the discussion in §2.2 for the role of Compton heating/cooling in the energy balance of the external atmospheric layers).

Under these assumptions, the coupled equations for the transfer of the two normal modes

take the form (see e.g. Gnedin & Pavlov 1974; Yahel 1980)

$$\begin{aligned} -y_G \mu \frac{df^1}{d\tau} &= \int K_s^{11} f^{1'} d\mu' + \int K_s^{21} f^{2'} d\mu' - k_s^1 f^1 + k_{ab}^1 \left(\frac{1}{2} b_\nu - f^1 \right) \\ -y_G \mu \frac{df^2}{d\tau} &= \int K_s^{22} f^{2'} d\mu' + \int K_s^{12} f^{1'} d\mu' - k_s^2 f^2 + k_{ab}^2 \left(\frac{1}{2} b_\nu - f^2 \right) \end{aligned} \quad (2)$$

where $y_G = \sqrt{1 - 2GM/Rc^2}$ is the gravitational redshift factor, R and M are the star mass and radius, $\mu = \mathbf{n} \cdot \mathbf{s} = \cos \theta$, $f^i(\tau, \mu, \nu) = c^2 I^i / 2h^4 \nu^3$ denotes the photon occupation number for the ordinary ($i = 1$) and extraordinary ($i = 2$) mode, I^i is the specific intensity, $b_\nu = c^2 B_\nu / 2h^4 \nu^3$, and B_ν is the Planck function. In equations (2) k_{ab}^i is the total free-free opacity,

$$k_s^i(\mu, \nu) = \sum_{j=1}^2 \int K_s^{ij} d\mu' \quad (3)$$

and $K_s^{ij}(\mu, \mu', \nu)$ is the probability that an incident photon, which has polarization \hat{e}^i and propagates in the direction μ , scatters into a direction μ' and polarization \hat{e}^j . All the quantities appearing in equations (2) are referred to the local observer, at rest on the star surface; the photon energy measured by an observer at infinity is given by $h\nu_\infty = y_G h\nu$. The integral terms appearing into equations (2) account for the scattering emissivities, and all opacity/emissivity coefficients are normalized to κ_{es} . The expressions for the opacities relevant to the present calculation are reported in appendix A.

2.2. Atmospheric Structure

Accretion atmosphere models are constructed by solving the transfer equations (2) coupled to the hydrostatic equilibrium and the energy equation. The hydrostatic balance is simply expressed as

$$\frac{dP}{d\tau} = \frac{GM}{y_G^2 R^2 \kappa_{es}}, \quad (4)$$

where $P = k\rho T / \mu_e m_p$ ($\mu_e \sim 1/2$ for completely ionized hydrogen) is the gas pressure and we consider only the case $L/L_{Edd} \ll 1$, where $L = L(\tau)$ is the luminosity measured by the local observer. Since in all our models the ram pressure of the accreting material, $1/2\rho v^2$, turns out to be much smaller than the thermal pressure, it has been neglected, together with the radiative force. In this limit equation (4) is immediately integrated, and gives the density as a function of depth

$$\rho = \frac{GMm_p}{2y_G^2 R^2 \kappa_{es}} \frac{\tau}{kT(\tau)}. \quad (5)$$

The energy balance just states that the net radiative cooling must equate the heating W_H supplied by accretion. The radiative energy exchange is obtained adding equations (2) together, after multiplying them by $(\hbar\omega)^3$, and integrating over angles and energies. Since we assumed

conservative scattering, its contribution to the energy balance clearly vanishes. However, as discussed in previous investigations (Alme, & Wilson 1973; ZTZT), Comptonization is ineffective in modifying the spectrum, but plays a crucial role in determining the temperature in the external, optically thin layers. Contrary to what happens in cooling atmospheres, the temperature profile shows a sudden rise (or “jump”) in the external, low-density layers where the heating produced by the incoming protons is mainly balanced by Compton cooling. Including Compton heating/cooling the energy equation becomes

$$k_P \left(\frac{aT^4}{2} - \frac{k_{am}^1}{k_P} U^1 - \frac{k_{am}^2}{k_P} U^2 \right) + (\Gamma - \Lambda)_C = \frac{W_H}{c\kappa_{es}} \quad (6)$$

where U^i is the radiation energy density of mode i and k_P , k_{am}^i are defined in strict analogy with the Planck and absorption mean opacities in the unmagnetized case. In evaluating the previous expression the approximated formula by Arons, Klein, & Lea (1987) for the Compton rate in a magnetized plasma, $(\Gamma - \Lambda)_C$, has been used.

The detailed expressions for the heating rate W_H and the stopping depth τ_B in a magnetized atmosphere are presented in appendix B.

3. Results

3.1. Numerical Method

The numerical calculation was performed adapting to radiative transfer in a magnetized medium the tangent-ray code developed by Zane, Turolla, Nobili, & Erna (1996) for one-dimensional, general-relativistic radiation transfer. The method performs an ordinary Λ -iteration for computing the scattering integrals. Schematically, the calculation proceeds as follows. First an initial temperature profile is specified (usually that of an unmagnetized model with similar parameters calculated by ZTZT) and the zero-th order approximation for f^1 , f^2 is computed solving equations (2) with no scattering emissivity. The boundary conditions for ingoing ($\mu < 0$) trajectories are $f^i = 0$ at $\tau = \tau_{min}$ while diffusive boundary conditions at $\tau = \tau_{max}$ were used for outgoing ($\mu > 0$) trajectories. The computed intensities are then used to evaluate the scattering integrals and the whole procedure is repeated, keeping the temperature profile unchanged. As soon as corrections on the intensities are small enough, new temperature and density profiles are obtained solving equations (6) and (5). The whole scheme is then iterated to convergence. Each model is completely characterized by the magnetic field strength, the total luminosity and the luminosity at τ_B , or, equivalently, by B and the heating rate W_H (see appendix B). Since the code solves the full transfer problem, it allows for the complete determination of the radiation field, including its angular dependence. This ensures a more accurate treatment of non-anisotropic radiative process with respect to angle-averaged, diffusion approximations. Owing to the gravitational redshift, the total accretion luminosity measured at infinity is related to the local luminosity at the top of the atmosphere by $L_\infty = y_G^2 L(0)$.

Models presented below were computed using a logarithmic grid with 300 equally-spaced depth points, 20 equally-spaced angular points and 48 energies. We explored a wide range of luminosities and considered two representative values of the magnetic field, $B = 10^{12}$ and 10^{13} G. The model parameters are reported in Table 1, together with the accretion rate

$$\dot{M} = L(0) \frac{[1 - L(\tau_B)/L(0)]}{\eta c^2}; \quad (7)$$

here $\eta = 1 - y_G$ is the relativistic efficiency. Since the values of τ_B and $\omega_{c,e,p}$ depend on B , the adopted boundaries in depth and energy vary from model to model. Typical values are $\tau_{max} \sim 10^2$ and $\tau_{min} \sim 10^{-6} - 10^{-8}$; the energy range goes from 0.16 eV to 5.45 keV. The angle-averaged effective depth is always $\gtrsim 100$ at τ_{max} and $\sim 10^{-5}$ at τ_{min} .

Convergence was generally achieved after 20–30 iterations with a fractional accuracy ~ 0.01 both in the hydrodynamical variables and in the radiation field. As a further check on the accuracy of our solutions, the luminosity evaluated numerically was compared with

$$L(\tau) \approx L(0) - [L(0) - L(\tau_B)] \frac{1 - [1 - (1 - v_{th}^4/v_{ff}^4)(\tau/\tau_B)]^{1/2}}{1 - v_{th}^4/v_{ff}^4} \quad (8)$$

which follows integrating the first gray moment equation

$$\frac{dL}{d\tau} = - \frac{4\pi R^2 f_A W_H}{y_G \kappa_{es}} \quad (9)$$

and provides an analytical expression for L at $\tau < \tau_B$ (see appendix B for notation). Within the range of validity of equation (8), the two values of L differ by less than 4%.

In all models $M = 1M_\odot$, $R = 6GM/c^2 \simeq 0.89 \times 10^6$ cm which correspond to $\tau_s \simeq 3.3$ (see equation [B2]). Only model A5, the unmagnetized one, was computed with $\tau_s \simeq 8$. One of the largest complication introduced by the presence of the magnetic field is the large-scale pattern of the accretion flow. In particular, when the accretion rate is small the way the spherically symmetric infalling plasma enters the magnetosphere is not fully understood as yet (see e.g. Blaes, & Madau 1993, Arons & Lea 1980). In order to bracket uncertainties, we assume a fiducial value for the fraction of the star surface covered by accretion, $f_A = 0.01$. We stress that this choice has no effect on the spectral properties of the emitted radiation and affects only the total luminosity, which scales linearly with f_A .

3.2. Emerging Spectra

The emergent spectra for models A1–A2 and A3–A4 are shown in figures 1 and 2, together with the blackbody at the NS effective temperature, T_{eff} . An unmagnetized model (A5) with similar luminosity is shown in figure 3. The corresponding temperature profiles are plotted in figure 4. Note that in all the plots the photon energy is already corrected for the gravitational

redshift, so the spectral distribution is shown as a function of the energy as observed at Earth. As it is apparent comparing the different curves (see also the solutions computed by ZTZT) the thermal stratification of the atmosphere shows the same general features (inner layers in LTE, outer region dominated by Comptonization) independently of B .

The sudden growth of T (up to $10^7 - 10^8$ K) that appears in the external layers is basically due to the fact that free-free cooling can not balance the heating produced by accretion at low densities. The temperature then rises until it reaches a value at which Compton cooling becomes efficient. This effect has been discussed by ZTZT and Zane, Turolla, & Treves (1998) in connection with unmagnetized atmospheres and they have shown that the temperature jump is located at the depth where the free-free and Compton thermal timescales become comparable, $t_{ff} \sim t_C$. In the magnetized case the situation is very similar, but now there are two relevant free-free timescales, $t_{ff}^{(1)}$ and $t_{ff}^{(2)}$, one for each mode. Comptonization becomes the dominant cooling process for $t_C \lesssim \min(t_{ff}^{(1)}, t_{ff}^{(2)})$ and gives rise to the large jump present in all accretion models. For some values of the model parameters, the region where $\rho = \rho_{vac}$ coincides with the photospheric region for both modes (see appendix A.3). In this case, vacuum effects can produce the peculiar “double jump” structure present in model A1, with the first (small) jump located at a depth where $t_{ff}^{(1)}/t_{ff}^{(2)} \sim 1$.

In order to compare our results with models available in the literature, some cooling atmospheres have been also computed setting $W_H = 0$ in equation (6); accordingly, the luminosity is now a constant. The emergent spectra for two such models (C1 and C2, see Table 1) show a good agreement with those computed by Shibanov *et al.* (1992) using the diffusion approximation.

We find that the spectral hardening at low luminosities, typical of unmagnetized atmospheres, is far less pronounced but still present up to field strengths $\sim 10^{13}$ G and tends to disappear at large enough luminosities. For comparison, with $L \sim 4 \times 10^{33}$ erg/s, the magnetized ($B = 10^{12}$ G) spectrum has negligible hardening while the hardening ratio is still ~ 1.6 in unmagnetized models of similar luminosity (ZTZT). The overall dependence of the continuum is not particularly sensitive to the value of the magnetic field, although the absorption feature at the proton cyclotron energy becomes more prominent with increasing B .

3.3. The Optical Excess

The most striking result emerging from our computations is that, although spectra from cooling and accreting H atmospheres are rather similar in the X-rays, they differ substantially at low energies. Below ~ 10 eV spectra from accreting atmospheres exhibit a soft excess with respect to the blackbody spectrum which is not shared by the cooling models. This feature, which is present also in the unmagnetized case, can be viewed as a distinctive spectral signature of a low-luminosity, accreting neutron star. The fact that it was not reported by ZTZT (and by previous investigators, see e.g. Alme, & Wilson 1973) is because they were mainly interested

in the shape of the X-ray continuum and their energy range was not large enough to cover the optical band; besides, some numerical problems, related to the moment formalism used to solve the transfer, prevented ZTZT to reach very low frequencies. The evidence of the soft excess is even more apparent in figures 5, 6 and 7 where synthetic spectra are plotted together with the best fitting blackbody in the X-ray band. The excess at two selected optical wavelengths ($\lambda = 3000, 6060$ Å, see discussion below), together with the temperature T_{fit} of the best-fitting blackbody in the X-ray band, are reported in Table 2.

The appearance of an optical excess in accreting models is related to the behaviour of the temperature, which is different from that of cooling models. The external layers are now hotter because Comptonization dominates the thermal balance there. The low energy tail of the spectrum decouples at a depth that corresponds to the (relatively) high temperatures near the jump, and emerges at infinity as a planckian at a temperature higher than T_{eff} . By decreasing the luminosity, the temperature jump moves at lower scattering depth and the frequency below which the spectrum exceeds the blackbody at T_{eff} becomes lower.

The presence of an optical excess has been reported in the spectrum of a few isolated, nearby pulsars (Pavlov, Stringfellow, & Córdova 1996) and, at lower luminosities, in the spectrum of the ONSs candidate RX J18563.5-3754. RX J18563.5-3754 was observed in the X-ray band with ROSAT (Walter, Wolk, & Neuhäuser 1996) and by HST at $\lambda = 3000$ and 6060 Å (Walter, & Matthews 1997). These multiwavelength observations made evident that the spectrum of RX J18563.5-3754 is more complex than a simple blackbody. The blackbody fit to PSPC data underpredicts the optical fluxes f_{3000} and f_{6060} by a factor 2.4 and 3.7 respectively (Walter, & Matthews 1997; see also Pavlov *et al.* 1996). Models of cooling atmospheres based on different chemical compositions also underestimate the optical fluxes (Pavlov *et al.* 1996), while models with two blackbody components or with a surface temperature variation may fit the f_{3000} flux. Recent spectra from non-magnetic atmospheres with Fe or Si-ash compositions (see Walter, & An 1998) may also provide a fit of both the X-ray and optical data, although these spectral models agree with those of Rajagopal, & Romani (1996) but not with those of Pavlov *et al.* (1996). Given the considerable latitude of the unknown parameters f_A , L , B , however, results presented here indicate that the full spectral energy distribution may be consistent with the picture of an accreting NS. We want also to note that all models computed here have a blackbody temperature higher than that required to fit the X-ray spectrum of RX J18563.5-3754 (see Table 2) and, although we are far from having explored the model parameter space, present results indicate that the excess decreases for decreasing luminosities. Although the optical identification of another isolated NS candidate, RX J0720.4-3125, still lacks a definite confirmation, it is interesting to note that the counterpart proposed by Kulkarni & van Kerkwijk (1998) also shows a similar excess.

3.4. Fraction of Polarization

The fraction of polarization strongly depends on the energy band and, in the presence of a temperature and density gradient, shows a variety of different behaviours (see figure 8). Its sign is determined by the competition between plasma and vacuum properties in the photospheric layers. However, independently of the model parameters, the degree of polarization crosses zero at the very vicinity of the proton cyclotron energy (see eq. [A10]), where the mode absorption coefficients cross each other. The bulk of the thermal emission from low-luminosity accreting NSs falls in the extreme UV/soft X-ray band, which is subject to strong interstellar absorption, making difficult their identification. It has been suggested that the detection of the non-thermal cyclotron emission feature at highest energies may be a distinguishing signature for most of these low-luminosity sources (Nelson, *et al.* 1995). Our results show that observations of the proton cyclotron line combined with measures of polarization may also provide a powerful tool to determine the magnetic field of the source, even in the absence of pulsations.

4. Discussion and Conclusions

We have discussed the spectral distribution of the radiation emitted by a static, plane-parallel atmosphere around a strongly magnetized neutron star which is heated by accretion. Synthetic spectra have been computed solving the full transfer problem in a magnetohydrodynamic plasma for several values of the accretion luminosity and of the star magnetic field. In particular, we explored the low luminosities ($L \sim 10^{30}\text{--}10^{33}$ erg/s), typical e.g. of isolated accreting NSs, and found that model spectra show a distinctive excess at low energies over the blackbody distribution which best-fits the X-rays. The energy $\hbar\omega_{ex}$ at which the spectrum rises depends both on the field strength and the luminosity, but for $B \approx 10^{12}\text{--}10^{13}$ G $\hbar\omega_{ex} \sim 10$ eV, so that the optical emission of an accreting, NS is enhanced with respect to what is expected extrapolating the X-ray spectrum to optical wavelengths. The presence of an optical/UV bump is due to the fact that the low-frequency radiation decouples at very low values of the scattering depth in layers where the gas is kept at larger temperatures by Compton heating. Since a hot outer zone is exhibited by accreting and not by cooling atmospheres, the optical excess becomes a distinctive spectral feature of NSs accreting at low rates.

Despite present results are useful in shedding some light on the emission properties of accreting, magnetized neutron stars, many points still need further clarification before the problem is fully understood and some of the assumptions on which our investigation was based deserve a further discussion. In this paper we have considered only fully ionized, pure hydrogen atmospheres. In the case of cooling NSs, the emitted spectra are strongly influenced by the chemical composition of the surface layers which results from the supernova explosion and the subsequent envelope fallback. Present uncertainties motivated several authors to compute cooling spectra for different abundances (see e.g. Miller, & Neuhäuser 1991; Miller 1992; Pavlov, *et al.*

1995; Rajagopal, Romani, & Miller 1997) and led to the suggestion that the comparison between observed and synthetic X-ray spectra may probe the chemistry of the NS crust (Pavlov, *et al.* 1996). The assumption of a pure hydrogen atmosphere, although crude, is not unreasonable for an accretion atmosphere. In this case, in fact, incoming protons and spallation by energetic particles in the magnetosphere may enrich the NS surface with light elements (mainly H) and, owing to the rapid sedimentation, these elements should dominate the photospheric layers (Bildsten, Salpeter, & Wasserman 1992).

Even in this simplified picture, however, the assumption of complete ionization may not provide an entirely realistic description. In a strongly magnetized plasma atomic binding is greatly enhanced, mainly for light elements. For a typical field of $\sim 10^{12}$ G, the ionization potentials for the hydrogen ground state are $\sim 100 - 300$ eV, moving the photoionization thresholds into the soft X-rays (see e.g. Ruderman 1972; Shibanov *et al.* 1992). The role of photoionization and of pressure ionization in a magnetized hydrogen atmosphere has been investigated by a number of authors (e.g. Ventura, Herold, Ruder, & Geyer 1992; Potekhin, & Pavlov 1997; Potekhin, Shibanov, & Ventura 1998). The neutral fraction, f_H , reaches a peak at densities ≈ 1 g/cm³ then decreases due to pressure ionization and turns out to be highly dependent on the temperature. While f_H never exceeds a few percent at $T = 10^6$ K, it becomes as large as $\sim 80\%$ for $T = 10^{5.5}$ K and $B = 10^{13}$ G. Although in the models we presented here such low temperatures are only reached in relatively low-density layers (see figure 4), hydrogen ionization equilibrium should be properly included in a more detailed analysis.

The effects of different orientations of the magnetic field through the atmosphere have been also neglected by keeping $\mathbf{B} \parallel \mathbf{n}$, a key simplifying assumption which allowed us to solve the transfer problem in one spatial dimension. Clearly, such an approximate description is valid only if the size of the emitting caps is small. Due to the intrinsic anisotropy of a magnetized medium, the emerging flux is expected to depend on the angle θ_B between the magnetic field and the normal to the surface. Shibanov *et al.* (1992) estimated that in a cooling atmosphere the flux at 1 keV from a surface element perpendicular to the field may exceed that of an element parallel to \mathbf{B} by nearly 50%. This result shows that a non-uniform magnetic field may lead to a significant distortion in the emerging spectra. Moreover, if the orientation of B varies along the atmosphere, tangential components of the radiative flux may induce some meridional circulation to maintain the heat balance (Kaminker, Pavlov, & Shibanov 1982).

When the finite size of the emitting regions is accounted for, the problem can not be reduced to a plane-parallel geometry and its solution necessarily demands for multidimensional transfer algorithms (e.g. Burnard, Klein, & Arons 1988, 1990; Hsu, Arons, & Klein 1997). Calculations performed so far were aimed to the solution of the frequency-dependent radiative problem on a fixed background or of the full radiation hydrodynamical problem in the frequency-integrated case. Numerical codes for the solution of the full transfer problem in axially symmetric media under general conditions are now available, see e.g. ZEUS (Stone, & Norman 1992), ALTAIR (Dykema, Castor, & Klein 1996) and RADICAL (Dullemond, & Turolla 1999). Their application

to the transfer of radiation in accretion atmospheres around magnetized NSs can add new insights on the properties of the emitted spectra.

We are grateful to G.G. Pavlov and to V.E. Zavlin for several very helpful discussions, and to A.Y. Potekhin for providing us with the expressions for the ion opacities. We also thank S. Rappaport for calling our attention to some useful references.

A. Radiative Processes in a Magnetized Medium

A.1. Electron Scattering

The electron contribution to the scattering source terms has been evaluated using the expression of the differential cross section, $d\sigma^{ij}/d\Omega$, discussed by Ventura (1979) and Kaminker, Pavlov, & Shibanov (1982). The electron contribution to K_s^{ij} can be simply written as

$$K_{s,e}^{ij} = \frac{1}{m_p \kappa_{es}} \int d\phi' \frac{d\sigma^{ij}}{d\Omega} \approx \frac{3}{4} \sum_{\alpha=-1}^1 |e_\alpha^{j'}|^2 |e_\alpha^i|^2 \frac{1}{(1 + \alpha u^{1/2})^2 + \gamma_r^2}. \quad (\text{A1})$$

where $u = \omega_{c,e}^2/\omega^2$, the e_α^i are the components of the normal mode unit polarization vector in a coordinate frame with the z -axis along \mathbf{B} and $\gamma_r = (2/3)(e^2/m_e c^3)\omega$ is the radiation damping. Further integration over θ' gives the total opacities

$$k_{s,e}^i = \sum_{j=1}^2 \int K_{s,e}^{ij} d\mu' \approx \sum_{\alpha=-1}^1 |e_\alpha^i|^2 \frac{1}{(1 + \alpha u^{1/2})^2 + \gamma_r^2}. \quad (\text{A2})$$

For energies near the proton cyclotron frequency $\omega_{c,p} = (m_e/m_p)\omega_{c,e}$, Thomson scattering on ions becomes important. The corresponding opacity has been derived by Pavlov *et al.* (1995) in a relaxation-time approximation and it is

$$K_{s,p}^{ij} \approx \frac{3}{4} \mu_m^2 \sum_{\alpha=-1}^1 |e_\alpha^{j'}|^2 |e_\alpha^i|^2 \frac{1}{(1 - \alpha u_p^{1/2})^2 + \mu_m^2 \gamma_r^2}. \quad (\text{A3})$$

$$k_{s,p}^i \approx \mu_m^2 \sum_{\alpha=-1}^1 |e_\alpha^i|^2 \frac{1}{(1 - \alpha u_p^{1/2})^2 + \mu_m^2 \gamma_r^2}, \quad (\text{A4})$$

where $\mu_m = m_e/m_p$ and $u_p = \omega_{c,p}^2/\omega^2$. The total opacities K_s^{ij} and k_s^i appearing in equations (2) are then evaluated by adding the contributions of the two species.

A.2. Bremsstrahlung

The electron and proton contributions to free–free opacity have a structure similar to that discussed for scattering. In a pure hydrogen plasma, they are given by (see Pavlov, & Panov 1976; Mészáros 1992; Pavlov *et al.* 1995)

$$k_{ab,e}^i \approx \frac{\kappa_{ff}}{\kappa_{es}} \sum_{\alpha=-1}^1 \left| e_\alpha^i \right|^2 \frac{g_\alpha}{(1 + \alpha u^{1/2})^2 + \gamma_r^2}, \quad (\text{A5})$$

$$k_{ab,p}^i \approx \frac{\kappa_{ff}}{\kappa_{es}} \mu_m^2 \sum_{\alpha=-1}^1 \left| e_\alpha^i \right|^2 \frac{g_\alpha}{(1 - \alpha u^{1/2})^2 + \mu_m^2 \gamma_r^2} \quad (\text{A6})$$

where

$$\kappa_{ff} = 4\pi^2 \alpha_F^3 \frac{\hbar^2 c^2}{m_e^2} \frac{n_e^2}{v_T \omega^3} [1 - \exp(-\hbar\omega/kT)], \quad (\text{A7})$$

$g_0 = g_{||}$, $g_{-1} = g_{+1} = g_\perp$, and $g_{||}$, g_\perp are the modified Gaunt factors, which account for the anisotropy induced by the magnetic field. The quantity κ_{ff} is the free–free opacity of a non–magnetic plasma apart from a factor $(4\pi/3\sqrt{3})g$, where g is the unmagnetized Gaunt factor. The total absorption opacity can be then evaluated by summing over the two species.

The modified Gaunt factors were computed evaluating numerically their integral form as given by Pavlov, & Panov (1976). At low temperatures and small frequencies ($u \gg 1$), where direct numerical quadrature becomes troublesome, the Gaunt factors have been obtained from the simpler formulas by Nagel (1980; see also Mészáros 1992; Rajagopal, Romani, & Miller 1997 and references therein). In order to decrease the computational time, the Gaunt factors have been evaluated once for all over a sufficiently large grid of temperatures and frequencies. In the transfer calculation they are then obtained at the required values of T and ω by polynomial interpolation.

A.3. Vacuum Effects and Mode Switching

The opacities of a real plasma start to change, due to the vacuum corrections in the polarization eigenmodes, when the field approaches the critical value $B_c = m_e^2 c^3 / \hbar e \simeq 4.41 \times 10^{13}$ G. The vacuum contribution has been included modifying the expressions for the e_α^i as discussed by Kaminker, Pavlov, & Shibanov (1982), and is controlled by the vacuum parameter W

$$W = \left(\frac{3 \times 10^{28} \text{ cm}^{-3}}{n_e} \right) \left(\frac{B}{B_c} \right)^4. \quad (\text{A8})$$

The inclusion of vacuum and of the protons produces the breakdown of the NM approximation near the mode collapse points (MCPs; see e.g. Pavlov, & Shibanov 1979; Mészáros 1992 and references therein). For $W > 4$, or $\rho < \rho_{vac} = 3.3 \times 10^{-3} (B/10^{12} \text{ G})^4 \text{ g/cm}^3$, the MCPs appear at the two critical frequencies

$$\omega_{c1,2}^2 = \frac{1}{2}\omega_{c,e}^2 \left[1 \pm \left(1 - \frac{4}{W} \right)^{1/2} \right]. \quad (\text{A9})$$

MCPs play an important role in the transfer of radiation through a magnetized medium, since the absorption coefficients of the two modes either cross each other or have a close approach, depending on the angle. Following the discussion by Pavlov, & Shibanov (1979), under the typical conditions at hand mode switching is likely to occur at nearly all values of μ . For this reason and for the sake of simplicity, in the present calculation we assumed mode switching for any value of μ at the two vacuum critical frequencies.

As shown by Bulik, & Pavlov (1996) in a fully ionized hydrogen plasma the presence of protons introduces (even in the absence of vacuum) a new MCP at

$$\omega_{c,3} = \frac{\omega_{c,p}}{\sqrt{1 - \omega_{c,p}/\omega_{c,e} + \omega_{c,p}^2/\omega_{c,e}^2}} \simeq \omega_{c,p} \left(1 + \frac{m_e}{2m_p} \right). \quad (\text{A10})$$

At $\omega = \omega_{c,3}$ the opacity coefficients cross (Zavlin, private communication), and the MCP related to the proton contribution is again a mode switching point. Although we are aware of no detailed calculation of the polarization modes in a “protons + electrons + vacuum” plasma, it seems natural to assume that, at least if $\omega_{c,2} > \omega_{c,3}$, the proton contribution to the “vacuum” term may be safely neglected, being a function of the ratio m_e/m_p .

B. Stopping Depth and Heating Rate in a Magnetized Atmosphere

In the unmagnetized case, under the assumption that all the proton stopping power is converted into electromagnetic radiation within the atmosphere, W_H can be approximated as (Alme, & Wilson 1973; ZTZT)

$$W_H \approx \begin{cases} \frac{y_G \kappa_{es}}{8\pi R^2 \tau_s f_A} [L(0) - L(\tau_s)] \frac{f(x_e)}{[1 - (1 - v_{th}^4/v_{ff}^4)(\tau/\tau_s)]^{1/2}} & \tau < \tau_s \\ 0 & \tau \geq \tau_s \end{cases} \quad (\text{B1})$$

where f_A is the fraction of the star surface covered by accretion, τ_s is the proton stopping depth and $v_{th}^2/v_{ff}^2 = 3kT(\tau_s)R/(2m_pGM)$ is the squared ratio of the proton thermal velocity to the free-fall velocity. For cold atmospheres in which the proton kinetic energy is much larger than the thermal energy, $f(x_e)$ can be safely taken to be unity for all practical purposes.

Infalling protons loose their energy to electrons via Coulomb collisions and the generation of collective plasma oscillations and τ_s can be approximated as (e.g. Zel'dovich, & Shakura 1969; Nelson, Salpeter, & Wasserman 1993)

$$\tau_s \approx \frac{1}{6} \frac{m_p}{m_e} \frac{v_{ff}^4}{c^4 \ln \Lambda_c} \simeq 2.6 \left(\frac{M}{M_\odot} \right)^2 \left(\frac{R}{10^6 \text{ cm}} \right)^{-2} \left(\frac{10}{\ln \Lambda_c} \right) \quad (\text{B2})$$

where $\ln \Lambda_c$ is a (constant) Coulomb logarithm.

The proton stopping process in strongly magnetized atmospheres presents a few differences, and has been discussed in detail by Nelson, Salpeter, & Wasserman (1993). Now the proton stopping depth, τ_B , is larger than τ_s , essentially because the magnetic field reduces the effective Coulomb logarithm perpendicular to the field. The expression for the proton stopping power retains, nevertheless, the same form as in the unmagnetized case. In the present calculation we used their approximate expression which relates τ_B to τ_s at different field strengths

$$\frac{\tau_B}{\tau_s} \approx \begin{cases} \frac{\ln \Lambda_c}{\ln(2n_{max})} & n_{max} \gtrsim 1 \\ 2 \ln(m_p/m_e) \simeq 15 & n_{max} \lesssim 1 \end{cases} \quad (B3)$$

$n_{max} = m_e v_{ff}^2 / (2\hbar\omega_{c,e}) \simeq 6.4(M/M_\odot)(R/10^6 \text{ cm})^{-1}(B/10^{12} \text{ G})^{-1}$. Since proton–proton interactions limit the stopping length to the mean-free path for nuclear collisions, which corresponds to $\tau_{pp} \sim 22$ (Mészáros 1992), if the value of τ_B which follows from equation (B3) exceeds τ_{pp} , the latter is used instead.

In the very strong field limit ($n_{max} \lesssim 1$), expression (B1) for the heating rate is still valid, provided that τ_s is replaced by τ_B . The situation is more complicated in the moderate field limit ($n_{max} \gtrsim 1$). In this case, not only τ_s must be replaced by τ_B , but a further effect must be accounted for. Now a sizeable fraction, $\sim 1 - 1/\ln(2n_{max})$, of the initial proton energy goes into excitations of electrons Landau levels. The cyclotron photons produced by radiative deexcitation will be partly thermalized by absorption and Compton scattering while the remaining ones escape forming a broad cyclotron emission feature (Nelson, *et al.* 1995). To account for this we take in the moderate field limit,

$$W_{MF} = (1 - f)W_H + fW_H(\Delta\epsilon/\epsilon) \quad (B4)$$

where f is the fraction of the initial proton energy which goes into Landau excitations and

$$\frac{\Delta\epsilon}{\epsilon} \approx \frac{(\hbar\omega_{c,e}/m_e c^2)\tau^2}{1 + (\hbar\omega_{c,e}/m_e c^2)\tau^2} \quad (B5)$$

is the electron fractional energy gain due to repeated scatterings. Strictly speaking, equation (B5) is valid only for photons produced below $\tau_C \sim (\hbar\omega_{c,e}/m_e c^2)^{-1/2} \simeq 7(B/10^{12} \text{ G})^{-1/2}$, because only these photons loose a significant fraction of their energy in Compton collisions with electrons. We have also to take into account that cyclotron photons produced at depths greater than the thermalization depth, $\tau_{th} \sim 16(B/10^{12} \text{ G})^{7/6}(M/M_\odot)^{1/3}(R/10^6 \text{ cm})^{2/3}(T/10^7 \text{ K})^{1/3}$, are absorbed. In our models, however, τ_B is always less than τ_{th} , so we do not need to worry about free–free absorption in (B4). A parabolic fit to the sum of first two curves ($0 \rightarrow 1$ and $0 \rightarrow 2$ Landau transitions) in figure 4 of Nelson, Salpeter, & Wasserman (1993) is very accurate and gives

$$f(\tau) = 6.1 \times 10^{-4} + 6.5 \times 10^{-2}(\tau/\tau_s) + 8.7 \times 10^{-3}(\tau/\tau_s)^2. \quad (B6)$$

Table 1. Model Parameters

Model	B 10^{12} G	L_∞ 10^{33} erg s $^{-1}$	$L(\tau_B)/L(0)$	\dot{M} 10^{12} g s $^{-1}$	f_A
A1	1	0.1	0.17	0.75	0.01
A2	1	3.7	0.25	25	0.01
A3	10	0.2	0.28	0.13	0.01
A4	10	6.3	0.33	38	0.01
A5	0	4.3	0.29	28	0.01
C1	1	0.2	1	0	1
C2	9	0.52	1	0	1

Note. — The first letter in the model identifier refers to accretion (“A”) or cooling (“C”) atmospheres.

Table 2. Predicted Excess

Model	$\frac{F_{6060}}{F_{6060}^{bb}}$	$\frac{F_{3000}}{F_{3000}^{bb}}$	T_{fit}^{bb} (keV)
A1	1.60	1.36	0.25
A2	3.05	1.44	0.43
A3	1.12	1.06	0.25
A4	3.44	2.21	0.57
A5	3.49	2.16	0.52

REFERENCES

Alme, W.L., & Wilson, J.R. 1973, *ApJ*, 186, 1015

Arons, J., & Lea, S.M. 1980, *ApJ*, 235, 1016

Arons, J., Klein, R.I., & Lea, S.M. 1987, *ApJ*, 312, 666

Bildsten, L., Salpeter, E.E., & Wasserman, I. 1992, *ApJ*, 384, 143

Blaes, O., & Madau, P. 1993, *ApJ*, 403, 690

Bulik, T., & Pavlov, G.G. 1996, *ApJ*, 469, 373

Burnard, D.J., Klein, R.I., & Arons, J. 1988, *ApJ*, 324, 1001

Burnard, D.J., Klein, R.I., & Arons, J. 1990, *ApJ*, 349, 262

Dullemond, C.P., & Turolla, R. 1999, *MNRAS*, submitted

Dykema, P.G., Klein, R.I., & Castor, J.I. 1996, *ApJ*, 457, 892

Gnedin, Yu.N., & Pavlov, G.G. 1974, *Sov. Phys. JETP*, 38, 903

Haberl, F., *et al.* 1997, *A&A*, 326, 662

Haberl, F., Motch, C., & Pietsch, W. 1998, *Astron. Nachr.*, 319, 97

Haberl, F., Pietsch, W., & Motch, C. 1999, *A&A*, in the press (astro-ph/9911159)

Hsu, J.J.L., Arons, J., & Klein, R.I. 1997, *ApJ*, 478, 663

Kaminker, A.D., Pavlov, G.G., & Shibanov, Yu.A. 1982, *Ap&SS*, 86, 249

Kulkarni, S.R., & van Kerkwijk, M.H. 1998, *ApJ*, 507, L49

Miller, M.C., & Neuhäuser, D. 1991, *MNRAS*, 253, 107

Miller, M.C. 1992, *MNRAS*, 255, 129

Mészáros, P. 1992, High-Energy Radiation from Magnetized Neutron Stars (Chicago: The University of Chicago Press)

Motch, C., *et al.* 1999, *A&A*, in the press (astro-ph/9907306)

Nagel, W. 1980, *ApJ*, 236, 904

Nelson, R.W., Salpeter, E.E., & Wasserman, I. 1993, *ApJ*, 418, 874

Nelson, R.W., Wang, C.L., Salpeter, E.E., & Wasserman, I. 1995, *ApJ*, 438, L99

Pavlov, G.G., & Panov, A.N. 1976, Sov. Phys. JETP, 44, 300

Pavlov, G.G., & Shibanov, Yu.A. 1979, Sov. Phys. JETP, 49, 741

Pavlov, G.G., Shibanov, Yu.A., Zavlin, V.E., & Meyer, R.D. 1995, in The Lives of Neutron Stars, M.A. Alpar, et al. eds. (Dordrecht: Kluwers)

Pavlov, G.G., Stringfellow, G.S., & Córdova, F.A. 1996, ApJ, 467, 370

Pavlov, G.G., Zavlin, V.E., Trümper, J., & Neuhäuser, R. 1996, ApJ, 472, L33

Potekhin, A.Y., & Pavlov, G.G. 1993, ApJ, 407, 330

Potekhin, A.Y., & Pavlov, G.G. 1997, ApJ, 483, 414

Potekhin, A.Y., Shibanov, Yu.A., & Ventura, J. 1998, in Neutron Stars and Pulsars, N. Shibasaki, et al. eds. (Tokyo: Universal Academy Press)

Rajagopal, M., & Romani, R.W. 1996, ApJ, 461, 327

Rajagopal, M., Romani, R.W., & Miller, M.C. 1997, ApJ, 479, 347

Rappaport, S., & van den Heuvel, E.P.J. 1982, Be Stars, M. Jaschek & H.G. Groth eds. (Dordrecht: Reidel)

Romani, R.W. 1987, ApJ, 313, 718

Ruderman, M.A. 1972, IAU Symposium 53, The Physics of Dense Matter, Boulder, CO

Schwone, A.D., et al. 1999, A&A, 341, L51

Shibanov, Yu.A., Zavlin, V.E., Pavlov, G.G., & Ventura, J. 1992, A&A, 266, 313

Stone, J.M., & Norman, M.L. 1992, ApJS, 80, 753

Treves, A., & Colpi, M. 1991, A&A, 241, 107

Treves, A., Turolla, R., Zane, S., & Colpi, M. 1999, PASP, submitted

van den Heuvel, E.P.J., & Rappaport, S. 1986, Physics of Be Stars, A. Slettebak & T. Snow eds. (Cambridge: Cambridge University Press)

Ventura, J. 1979, Phys. Rev. D, 19, 1684

Ventura, J., Herold, H., Ruder, H. & Geyer, F. 1992, A&A, 261, 235

Walter, F.M., Wolk, S.J., & Neuhäuser, R. 1996, Nature, 379, 233

Walter, F.M., & Matthews, L.D. 1997, Nature, 389, 358

Walter, F.M., & An, P. 1998, 192nd AAS meeting, invited talk

Yahel, R.Z. 1980, ApJ, 236, 911

Zampieri, L., Turolla, R., Zane, S., & Treves, A. 1995, ApJ, 439, 849 (ZTZT)

Zane, S., Turolla, R., Nobili, L., & Erna, M. 1996, ApJ, 466, 871

Zane, S., Turolla, R., & Treves, A. 1998, ApJ, 501, 258

Zel'dovich, Ya., & Shakura, N. 1969, Soviet Astron.–AJ, 13, 175

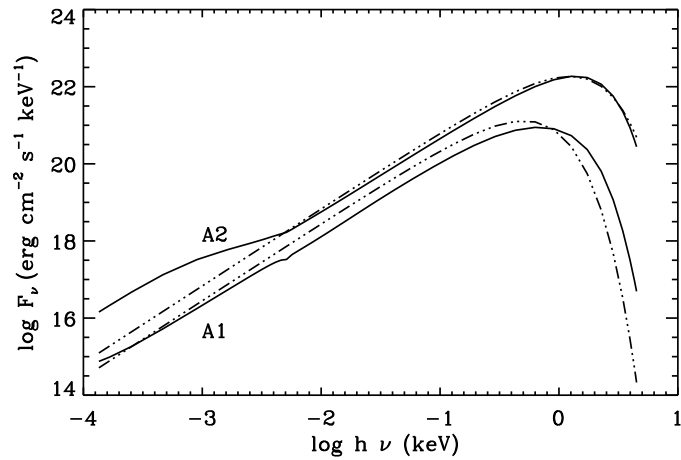


Fig. 1.— Emergent spectra for models A1 and A2 (full lines), together with the blackbody spectra at the neutron star effective temperature (dash-dotted lines).

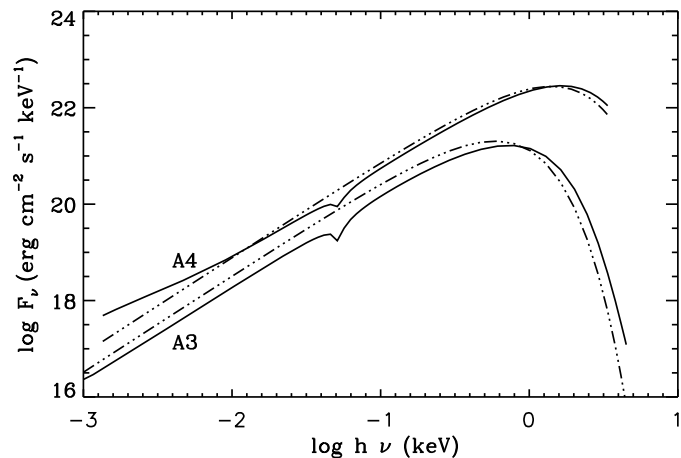


Fig. 2.— Same as in figure 1 for models A3 and A4.

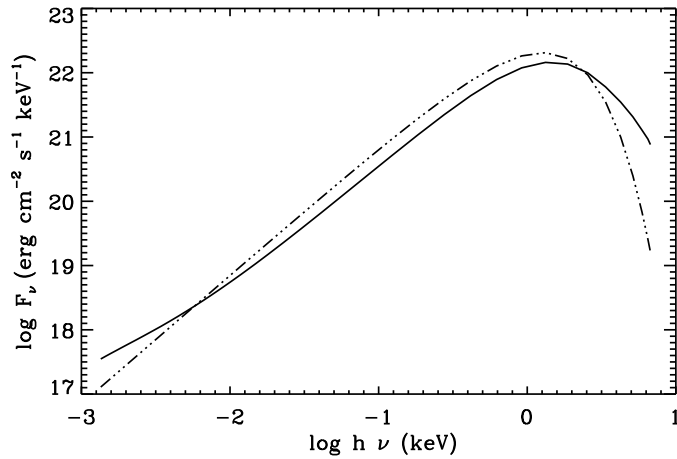


Fig. 3.— Same as in figure 1 for $B = 0$ (model A5).

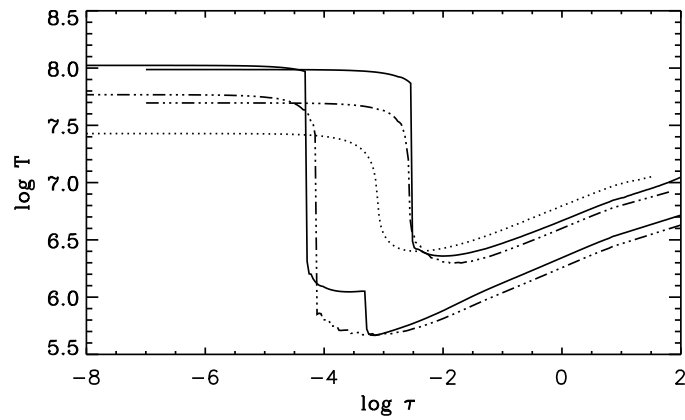


Fig. 4.— The run of the gas temperature in the atmosphere for the models of figures 1, 2 and 3; solid lines correspond to $B = 10^{12}$ G, dash-dotted lines to $B = 10^{13}$ G and dotted lines to $B = 0$.

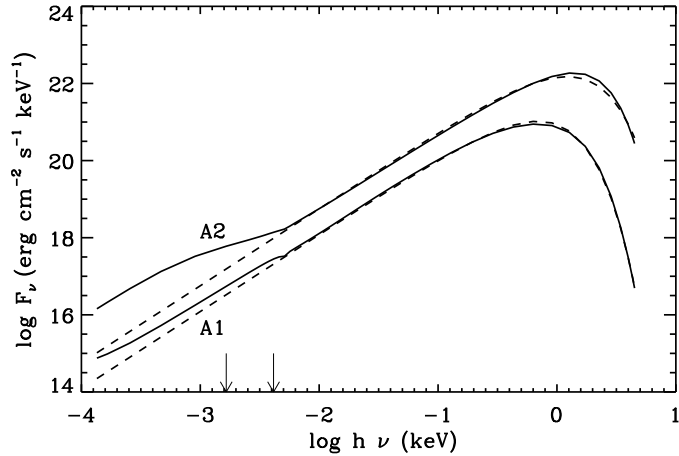


Fig. 5.— Same models as in figure 1, together with the two blackbody functions which best-fit the X-ray spectra in the 0.03–4.5 keV interval (dashed lines). The arrows mark the 3000–7500 Å band.

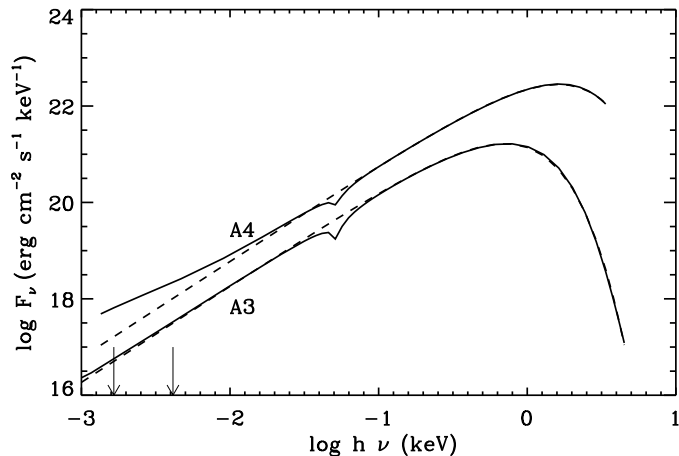


Fig. 6.— Same as in figure 5, for the models with $B = 10^{13}$ G; here the fit is computed in the 0.19–3.4/4.5 keV band for the two solutions.

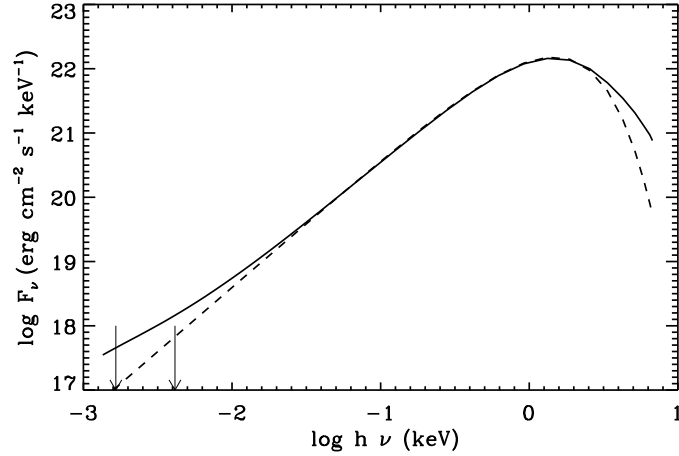


Fig. 7.— Same as in figure 5, for the models with $B = 0$; here the fit is computed in the 0.02–3.3 keV band.

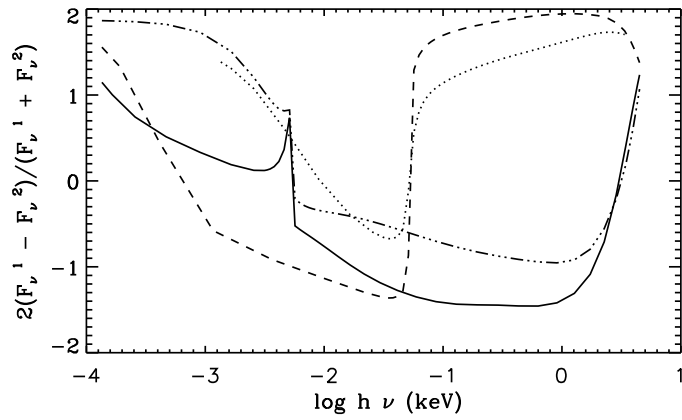


Fig. 8.— Fraction of polarization for the same models as in figures 1 and 2. Solid line: model A1; dash-dotted line: A2; dotted line: A3; dashed line: A4.